Isoscalar $E0-E3$ strength in ^{116}Sn, ^{144}Sm, ^{154}Sm, and ^{208}Pb

D. H. Youngblood, Y.-W. Lui, H. L. Clark, B. John,* Y. Tokimoto, and X. Chen
Cyclotron Institute, Texas A&M University, College Station, Texas 77840, USA
(Received 18 November 2003; published 11 March 2004)

The giant resonance region from 10 MeV$<E_x<$55 MeV in ^{116}Sn, ^{144}Sm, ^{154}Sm, and ^{208}Pb has been studied with inelastic scattering of 240 MeV α particles at small angles including 0°. Essentially all of the expected isoscalar $E0$, $E1$, $E2$, and $E3$ strength was identified in these nuclei.

DOI: 10.1103/PhysRevC.69.034315 PACS number(s): 25.55.Ci, 24.30.Cz, 27.60.+j, 27.70.+q

I. INTRODUCTION

Isoscalar giant resonances have been extensively studied since the discovery of the isoscalar quadrupole resonance (GQR) in the early 1970s [1] and most of the isoscalar quadrupole strength in heavier nuclei was identified in early studies [2,3]. The isoscalar octupole resonance consists of $1\hbar\omega$ and $3\hbar\omega$ components [3,4], dubbed the low energy octupole (LEOR) and high energy octupole resonances (HEOR). There have been several studies of the LEOR as well as several reports of the HEOR [4]. The isoscalar giant monopole resonance (GMR), of particular interest since its energy can be directly related to the nuclear compressibility [5], was identified in 1977 [6] and was the subject of a number of studies through the 1980s [3,7]. The isoscalar giant dipole resonance (ISGDR) was first tentatively reported by Morsch *et al.* [8] in ^{208}Pb and a definitive identification was made by Davis *et al.* [9], also in ^{208}Pb. Like the GMR, the ISGDR is a compression mode [10] and provides information about the nuclear compressibility from which the compressibility of nuclear matter (K_{NM}) can be obtained [5]. Most of these works used inelastic α scattering (partly to suppress excitation of isovector states) with energies from 96 to 175 MeV. The highest α energy used in studies that included the 0° scattering necessary to definitively identify the GMR was 130 MeV. In most cases, the strength of a particular giant resonance was assumed to be collected in a narrow region with a Guassian or Lorentzian shape, and multiple Guassians were fit to data at different angles to extract giant resonance parameters.

In the last several years, we have carried out (α,α') studies of many nuclei at 240 MeV and measured inelastic scattering into 0° to extract $E0$ strength distributions and determine the incompressibility of nuclear matter. We have previously reported $E0$ strength distributions in ^{90}Zr, ^{116}Sn, ^{144}Sm, and ^{208}Pb [11] as well as $E0$ and $E2$ distributions for the deformed nucleus ^{154}Sm [12] and isoscalar $E1$ distributions in ^{90}Zr, ^{116}Sn, and ^{208}Pb [13], where the observation of a low energy component of the isoscalar giant dipole resonance was reported for the first time. The studies at 240 MeV have a much better peak to continuum ratio than the earlier studies, and we have been able to extract actual strength distributions for the various multipoles, without any *a priori* assumption about their distribution. In lighter nuclei (^{24}Mg, ^{28}Si, ^{40}Ca, ^{58}Ni) where earlier studies missed much of the $E0$ and $E2$ strength, we have been able to identify essentially all of the GMR and GQR strength [14]. M. Itoh *et al.* [15] and M. Uchida *et al.* [16] have also recently reported studies of the isoscalar resonances in the Sm isotopes and ^{208}Pb with 400 MeV α particles.

We report here a systematic analysis which identifies isoscalar $E0$, $E1$, $E2$, and $E3$ strength between $10<E_x<35$ MeV in ^{116}Sn, ^{144}Sm, ^{154}Sm, and ^{208}Pb. For calculations with the distorted wave Born approximation

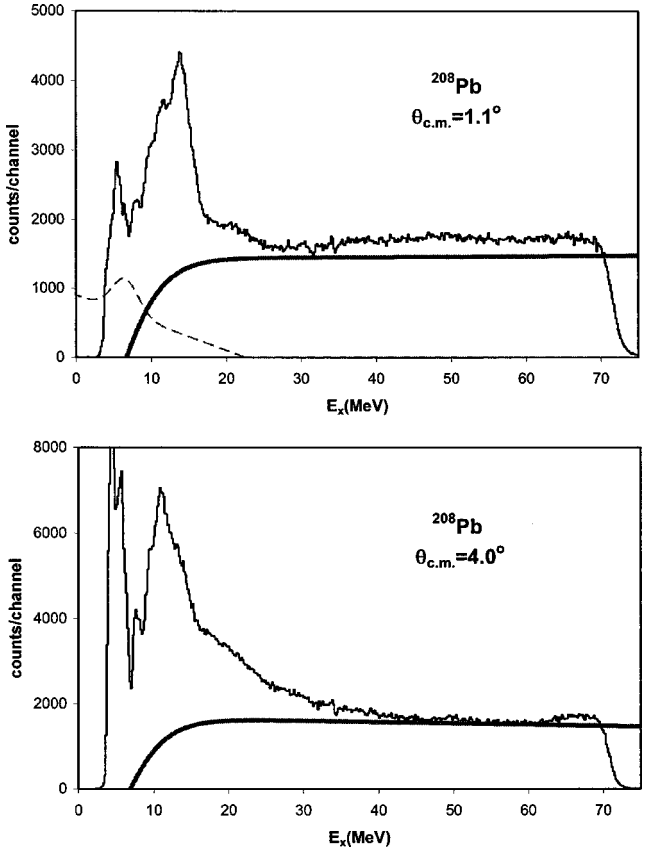

FIG. 1. Inelastic α spectra obtained at two angles for ^{208}Pb. The thick gray lines show the continuum chosen for the analysis. The dashed line below 22 MeV represents a contaminant present at some angles in the spectra taken with the spectrometer at 0°. This was subtracted before the multipole analysis was done.

*Present address: Nuclear Physics Division, Bhabha Atomic Research Center, Mumbai-400085, India.

 ©2004 The American Physical Society

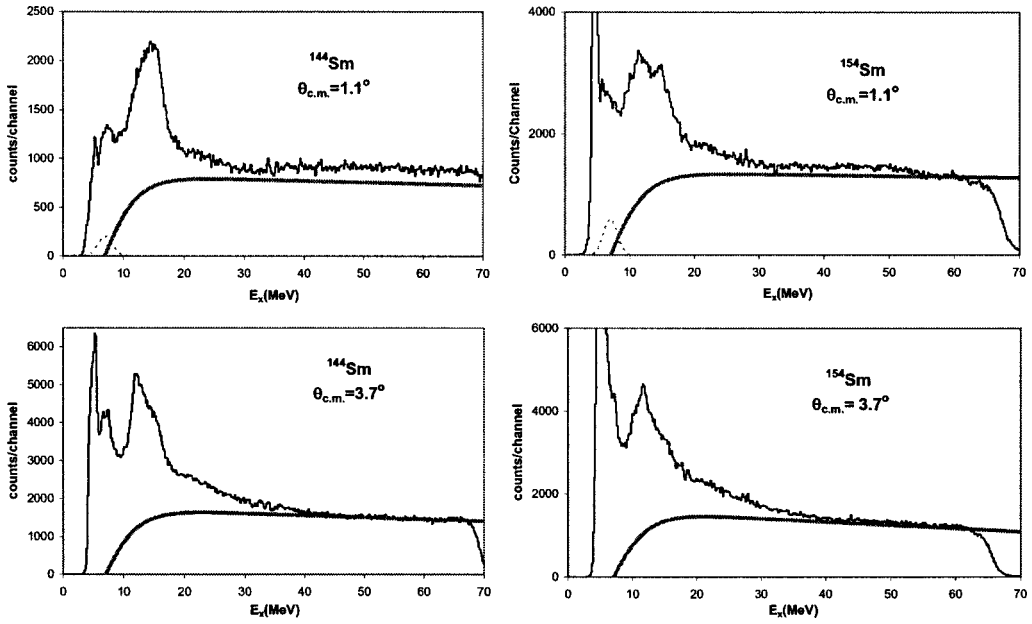

FIG. 2. Inelastic α spectra obtained for ^{144}Sm and ^{154}Sm. The thick gray lines show the continuum chosen for the analysis. The dashed line below 10 MeV represents a contaminant peak present at some angles in the spectra taken with the spectrometer at 0°. This was subtracted before the multipole analysis was done.

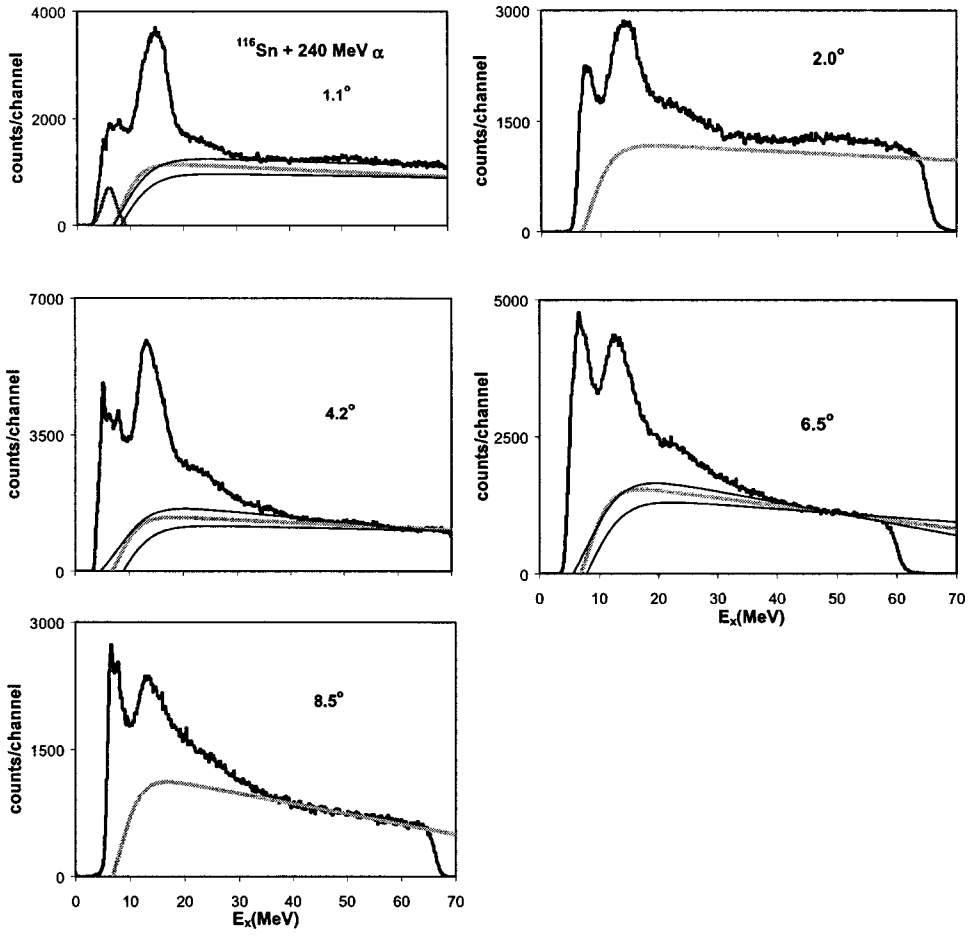

FIG. 3. Inelastic α spectra obtained at several angles for ^{116}Sn. The thick gray lines show the continuum chosen for the analysis. Thin black lines in three of the spectra indicate the extent of variation of the continuum as discussed in the text. The dashed line below 10 MeV in the 1.1° spectrum represents a contaminant peak present at some angles in the spectra taken with the spectrometer at 0°. This was subtracted before the multipole analysis was done.

TABLE I. Optical and Fermi parameters used in DWBA calculations.

	V (MeV)	V_i (MeV)	r_i (fm)	a_i (fm)	c (fm)	a (fm)
^{116}Sn	36.7	23.94	0.998	1.047	5.433	0.515
^{144}Sm	43.2	34.93	0.958	0.963	5.850	0.525
^{208}Pb	43.3	61.40	1.032	0.567	6.670	0.545
^{154}Sm	43.2	34.93	0.958	0.963	6.107	0.523

(DWBA) we have used the folding model which provides transition strengths in agreement with electromagnetic values for $L=2,3,4$ transitions [14,17] rather than the deformed potential model used in most previous studies.

II. EXPERIMENTAL TECHNIQUE

The experimental technique has been described thoroughly in Ref. [14] and is summarized briefly below. Beams of 240 MeV α particles from the Texas A&M K500 superconducting cyclotron bombarded self-supporting foils, each enriched to more than 96% in the desired isotope, located in the target chamber of the multipole-dipole-multipole spectrometer. The horizontal acceptance of the spectrometer was 4° and ray tracing was used to reconstruct the scattering angle. The vertical acceptance was set at ±2°. The focal plane detector measured position and angle in the scattering plane and covered from $E_x \sim 8$ MeV to $E_x > 55$ MeV, depending on scattering angle. The out-of-plane scattering angle was not measured so the average scattering angle was obtained by integrating over the vertical opening. Position resolution of approximately 0.9 mm and scattering angle resolution of about 0.09° were obtained. At $\theta_{\mathrm{spec}}=0°$, runs with an empty target frame had an α-particle rate approximately $1/2000$ of that with a target in place and α particles were uniformly distributed in the spectrum. Cross sections were obtained from the charge collected, target thickness, dead time, and known solid angle. The target thickness's were measured by weighing and checked by measuring the

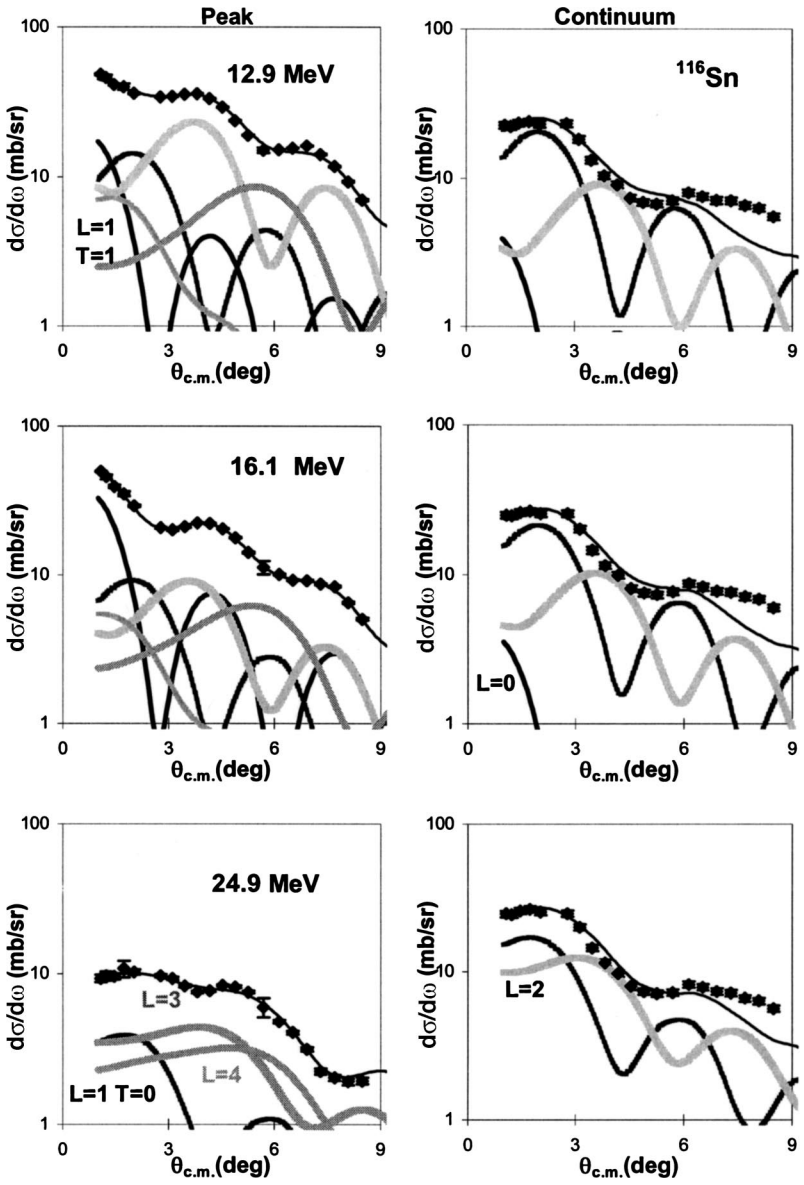

FIG. 4. The angular distributions of the ^{116}Sn cross sections for a 800 keV wide bin centered at the excitation energy indicated on the figure for inelastic α scattering for three excitation ranges of the GR peak and the continuum. The lines through the data points indicate the multipole fits. Contributions of each multipole are shown. Where errors are not shown, they are smaller than the data points.

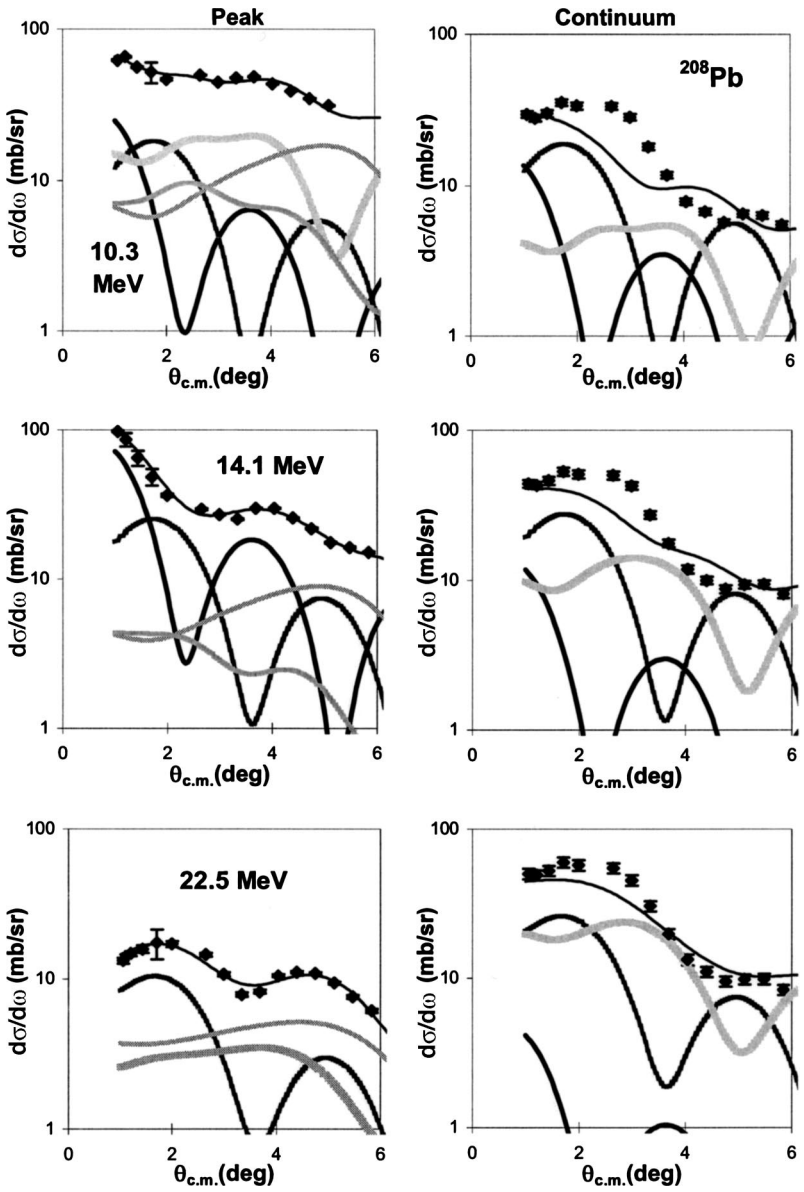

FIG. 5. The angular distributions of the ^{208}Pb cross sections for a 640 keV wide bin centered at the excitation energy indicated on the figure for inelastic α scattering for three excitation ranges of the GR peak and the continuum. The lines through the data points indicate the multipole fits. Contributions of each multipole are shown with the same line types as in Fig. 4. Where errors are not shown, they are smaller than the data points.

energy loss of the 240 MeV α beam in each target. The cumulative uncertainties in target thickness, solid angle, etc., result in about a ±10% uncertainty in absolute cross sections. ^{24}Mg spectra were taken before and after each run with each target and the 13.85±.02 MeV $L=0$ state [18] was used as a check on the calibration in the giant resonance region.

Most of the data have already been reported in Refs. [11–13] and several spectra are shown in these works. These data were taken at spectrometer angles 0° and 4°. Additional data is included in this work that in some cases improved the statistics and in other cases provided additional angles. In particular, additional data were taken for ^{116}Sn with the spectrometer at 6° extending the measurement range to the c.m. angle 8.5°. Examples of a typical set of giant resonance spectra obtained for ^{208}Pb are shown in Fig. 1 and for ^{144}Sm and ^{154}Sm in Fig. 2. At higher excitation, these spectra appear to consist of a sharp (few MeV wide) peak sitting on a broad peak (15–20 MeV wide), then blending into a continuum around E_x=40 MeV. The shape and relative strengths of both the sharp and broad peaks change as a function of angle. Samples of ^{116}Sn spectra obtained for average c.m. angles from 1.1° to 8.5° are shown in Fig. 3.

III. DATA ANALYSIS

For this study we carried out density dependent single folding DWBA calculations as described by Satchler and Khoa [19]. Using such calculations, analyses of 240 MeV inelastic α-particle scattering exciting low lying states in ^{24}Mg and ^{28}Si [14] have been shown to give B(EL) values in agreement with values obtained from electromagnetic probes. Optical parameters for the calculations were determined from elastic scattering for ^{116}Sn [20], ^{144}Sm [21], and ^{208}Pb [21] and are given in Table I along with the Fermi parameters of the density distribution of the nuclear ground state. For each nucleus, B(EL) values obtained from inelastic α scattering for low lying states agreed with electromagnetic values. Elastic scattering data were not available for ^{154}Sm, so the parameters obtained for ^{144}Sm were used. The transition densities, sum rules, and DWBA calculations were dis-

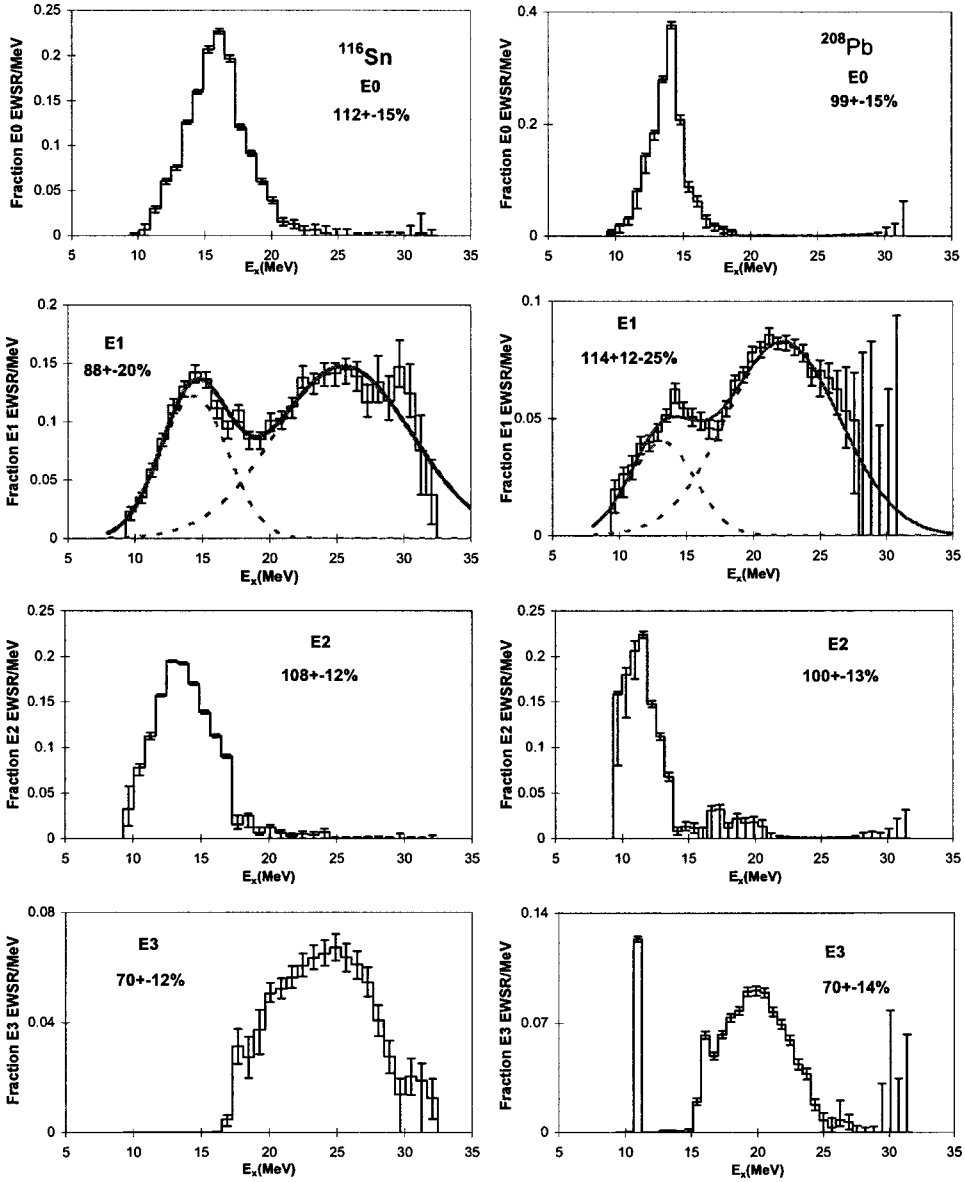

FIG. 6. Strength distributions obtained from the peak analysis for ^{116}Sn and ^{208}Pb are shown by the histograms. Error bars represent the uncertainty due to the fitting of the angular distributions and different choices of the continuum as described in the text. The lines on the $E1$ distribution represent Gaussians calculated with the parameters in Table III.

cussed thoroughly in Ref. [22] and, except for the isoscalar dipole resonance, the same expressions and techniques were used in this work. The isoscalar dipole transition density given by Harakeh and Dieperink [23] (and described in Ref. [22]) is for only one magnetic substate, so that the transition density given in Ref. [23] must be multiplied by the square root of 3 to represent inelastic α-particle excitation of the ISGDR. The analyses reported in Refs. [11,12] used the deformed potential model, which is known [17] to give B(EL) values in disagreement with electromagnetic probes.

The analysis techniques used were described in detail in Ref. [14]. Each spectrum was divided into a peak and a continuum where the continuum was assumed to have the shape of a straight line at high excitation joining onto a Fermi shape at low excitation to model particle threshold effects. Samples of the continua used are shown in Figs. 1–3. The multipole components of the giant resonance peak and the continuum were obtained by dividing the peak cross sections and continuum cross sections into multiple regions (bins) by excitation energy and then comparing the angular distributions obtained for each of these bins to DWBA calculations. The strengths of the isoscalar $E0$, $E1$, $E2$, $E3$, and $E4$ contributions were varied to minimize χ^2. For each nucleus the known isovector dipole strength distribution [24] was used to calculate the isovector giant dipole resonance (IVGDR) contribution and it was not varied. The uncertainty for the multipole fits was determined for each multipole by incrementing (or decrementing) that strength, then adjusting the strengths of the other multipoles to minimize total χ^2. This continued until the new χ^2 was 1 unit larger than the total χ^2 obtained for the best fit. In general our data do not go out far enough in angle to distinguish $E4$ from higher multipoles. However $L=4$ and higher multipoles are expected to be broadly distributed.

A number of analyses were carried out for each nucleus to assess the effects of different choices of the continuum on the resulting multipole distributions. Analyses were made using continua chosen with several different criteria [e.g., (a) using a slope for the linear part which did not quite match the data at high excitation; (b) lowering the continua so that

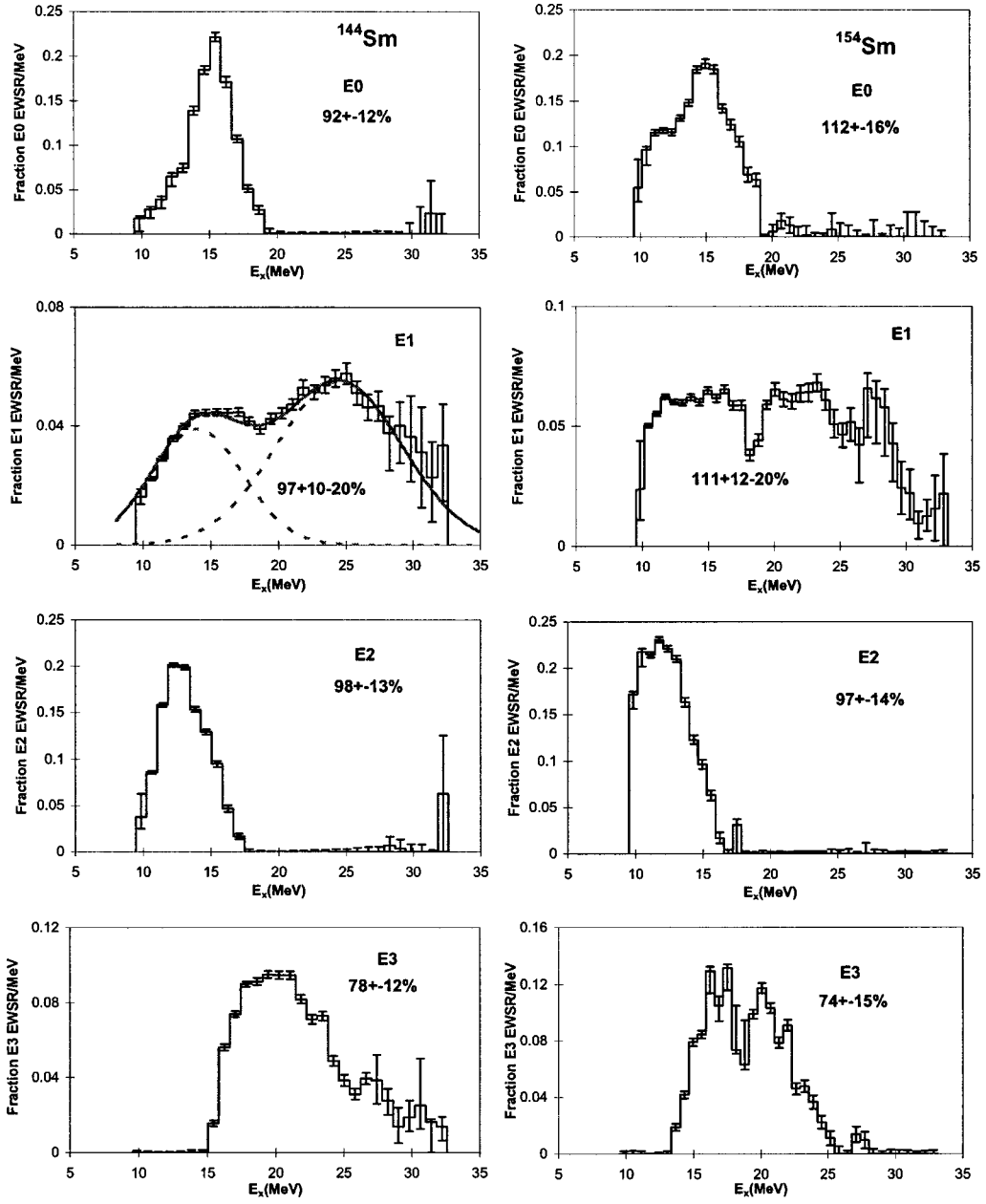

FIG. 7. Strength distributions obtained from the peak analysis for ^{144}Sm and ^{154}Sm are shown by the histograms. Error bars represent the uncertainty due to the fitting of the angular distributions and different choices of the continuum as described in the text. The lines on the $E1$ distribution for ^{144}Sm represent Gaussians calculated with the parameters in Table III.

it was always below the data; (c) changing the low energy cutoff and slope of the continuum; and (d) deliberately altering the continuum slope and/or amplitude at only selected angles]. The range of continua explored is indicated in Fig. 3 for three of the ^{116}Sn spectra. In most of the analyses, similar modifications were made to the continua at all angles (e.g., lowering the continuum at all angles), but the effects of different assumptions about the continua for spectra taken at different spectrometer angles were also explored (e.g., lowering the continuum for data taken with the spectrometer at 0°, and raising it for data taken at 4°). As these analyses produced a large number of distributions for each multipole, the distributions presented are the result of a weighted average of the distributions obtained with the different continua and the errors shown on the multipole distributions in Figs. 6 and 7 were obtained by adding the standard deviations between the results obtained from the different continua choices to the errors obtained from the multipole fits in quadrature. In general the $E0$ and lower part of the $E2$ distributions were relatively insensitive to the continuum choices while the $E1$ and $E3$ distributions were more dependent on the continuum choices. This is reflected in the errors on the multipole distributions with the $E1$ distributions having the largest errors, and somewhat smaller errors on the $E3$ distributions. The errors on the $E0$ and $E2$ distributions are the smallest. The errors obtained in the multipole fits for a given continuum are approximately the same for each multipolarity (they are a little larger for the $E1$ distribution), so

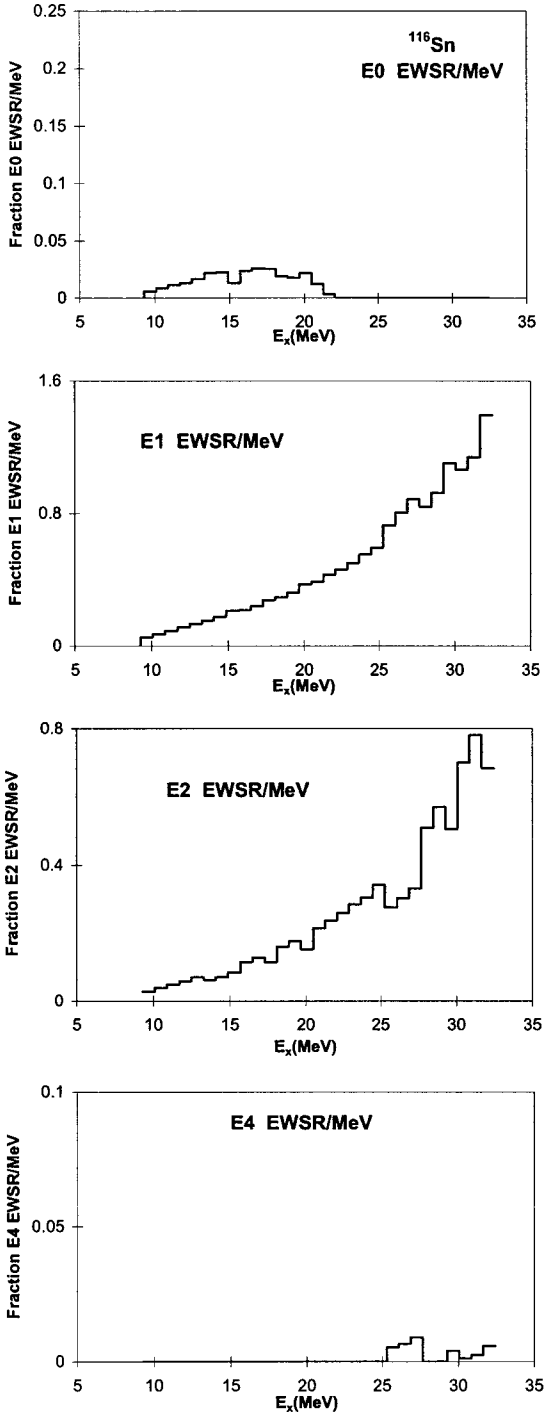

FIG. 8. Strength distributions obtained from analysis of the continuum for ^{116}Sn are shown by the histograms.

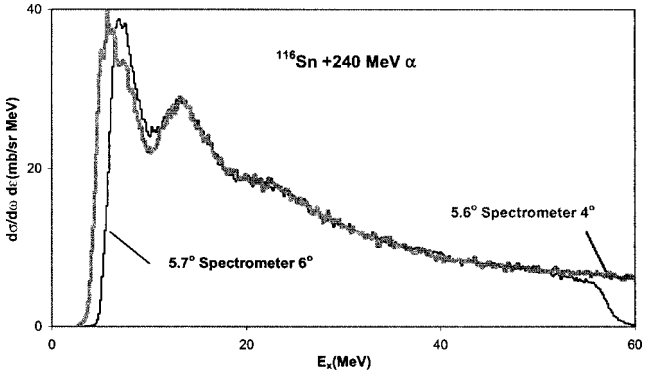

FIG. 9. Inelastic α spectra for ^{116}Sn obtained at $\theta_{\mathrm{c.m.}} \sim 5.7°$ in two runs at different spectrometer angles.

that most of the difference is due to the effects of differing continuum choices.

A sample of the angular distributions obtained for the giant resonance peak and the continuum are shown for ^{116}Sn and ^{208}Pb in Figs. 4 and 5 along with the DWBA fits. For both nuclei, the angular distributions of the cross sections for the giant resonance peak change dramatically with excitation energy, whereas those for the continuum are virtually the same over the entire energy range. The $E0$, $E1$, $E2$, and $E3$ distributions obtained for the peak from the DWBA fits are shown in Figs. 6 and 7. In all cases the $E2$ distributions are limited to a narrow peak at about $E_x = 62/A^{1/3}$ MeV and contain approximately 100% of the $E2$ energy weighted sum rule (EWSR), in agreement with previous works. The $E0$ distributions are peaked around $E_x = 66/A^{1/3}$ MeV but in ^{90}Zr the $E0$ distribution extends up to around $E_x = 25$ MeV (as reported in Ref. [11]), whereas in the other nuclei the $E0$ strength is limited to a narrow peak. In each case approximately 100% of the $E0$ EWSR is observed. The centroids of the $E3$ distributions are approximately at $93/A^{1/3}$ MeV, and around 75% of the strength is identified, consistent with approximately 25% of the $E3$ strength expected in $1\,\hbar\omega$ strength including the low energy octupole resonance [3]. The isoscalar $E1$ strength is split into an upper component ($E_x \sim 109/A^{1/3}$ MeV) and a lower component ($E_x \sim 63/A^{1/3}$MeV) and within errors 100% of the $E1$ EWSR was identified in each nucleus.

The general features of the continuum choices that led to these results can be seen in Figs. 1–3. The continua for all angles are similar, except that at the larger angles the slope is somewhat larger to match the data at high excitation. The first two spectra shown in Fig. 3 ($\theta_{\mathrm{av}} = 1.1°$ and $\theta_{\mathrm{av}} = 2.0°$ taken with the spectrometer at 0°) appear to have a broad peak above $E_x = 40$ MeV that is not present in the spectra taken with the spectrometer at larger angles. The origin of this peak is not known but could be due to the pickup breakup reactions (α,^{5}He$\rightarrow\alpha+n$) and (α,^{5}Li$\rightarrow\alpha+p$) which are particularly strong near 0° in 130 MeV inelastic α scattering [25]. There may also be real background contributions from scattering off of the θ and φ slits which are at 2°.

As can be seen in Figs. 4 and 5, the multipole fits to the continuum angular distributions are fair for ^{116}Sn and very poor for ^{208}Pb, suggesting that the data is not well represented by $E0$-$E4$ multipole transitions. The fits to the continuum distributions for ^{144,154}Sm are similar in quality to the ^{116}Sn fits. The "$E0$," "$E1$," "$E2$," and "$E4$" distributions (no $L=3$ strength was required to fit the continuum distributions) obtained from the fits to the continuum distributions are shown for ^{116}Sn in Fig. 8. For all the targets, the continuum distributions are fit primarily by $L=1$ and $L=2$ angular distributions, with some small amount $L=0$ at lower excitation and in some cases $L=4$ at higher excitation. This continuum "$E1$" and "$E2$" strength corresponds to many times the EWSR's for each of the nuclei and hence (most of it) cannot

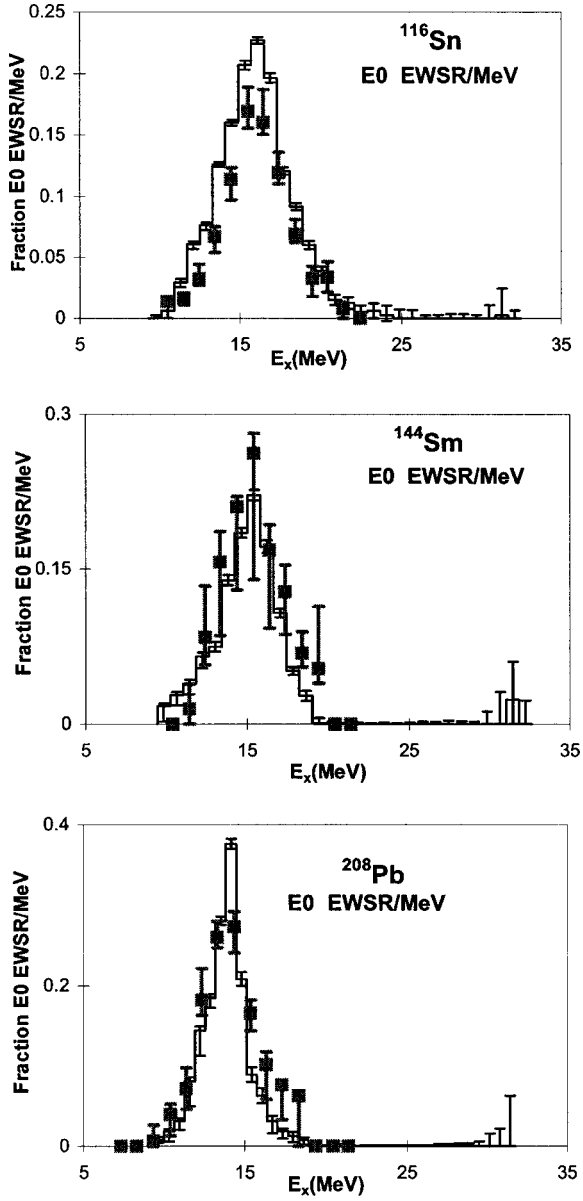

FIG. 10. $E0$ strength distributions obtained in this work are shown as black histograms and compared to those from Ref. [11], shown in gray.

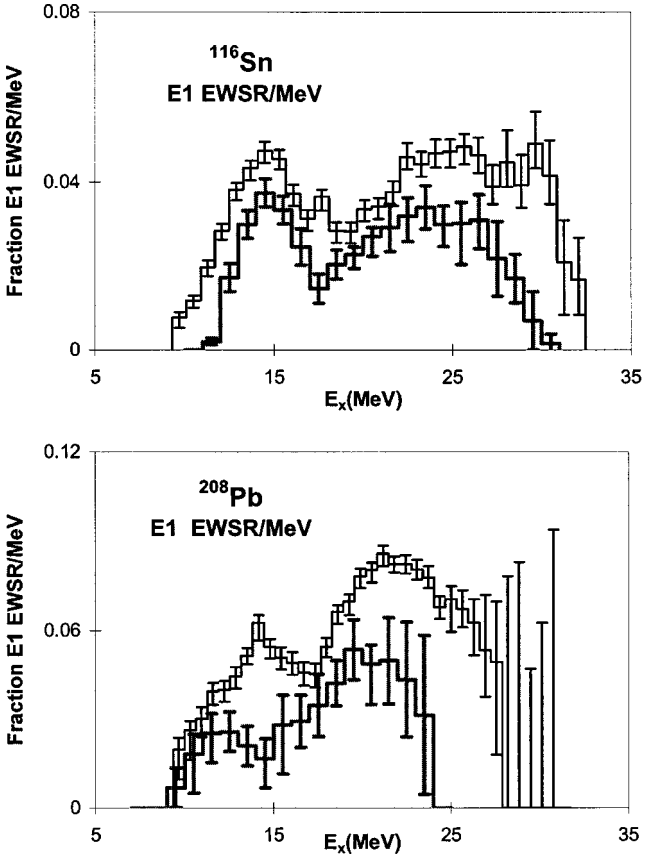

FIG. 11. $E1$ strength distributions obtained in this work are shown as black histograms and compared to those from Ref. [13], shown in gray. The vertical scales of the $E1$ distributions from Ref. [13] have been divided by three as discussed in the text.

be due to inelastic excitation of $E1$ or $E2$ strength in the target nuclei. As the quality of the fits is not good, the small "$E0$" and "$E4$" contributions also cannot be ascribed to multipole processes.

There are several physics processes that can contribute to the (apparent) inelastic α cross section. These include multipole excitations of the target nucleus, more complex multistep excitations, excitations of noncollective states, quasielastic scattering from target nucleons or clusters and pickup breakup reactions. Except for the lower multipole excitations, the other nuclear processes might be expected to form a continuum of real physics on which the lower multipole peaks sit. The pickup breakup reactions $(\alpha, {}^5\mathrm{He} \rightarrow \alpha + n)$ and $(\alpha, {}^5\mathrm{Li} \rightarrow \alpha + p)$ would result in broad peaks above an equivalent $E_x = 35$ MeV. In addition there is a real background in some of the spectra due to scattering off of the slits at the entrance to the spectrometer. In the spectra obtained with the spectrometer at 4°, there should be some experimental background in the spectra for the smallest angles ($\theta_{\mathrm{c.m.}} = 2.8°$) where scattering off the edge of the slit at $\theta_{\mathrm{lab}} = 2°$ causes a continuous (in E) contribution decreasing at larger E_x. With the spectrometer at 6.5°, a similar experimental background is expected at the smallest angle ($\theta_{\mathrm{c.m.}} = 5.3°$). Figure 9 compares spectra obtained for ^{116}Sn at similar angles not near a slit edge, but taken with the spectrometer at 4° and 6°. The spectra are in good agreement except near the low and high energy cutoffs where the detector response depends on spectrometer angle, suggesting that there is little experimental background in these spectra. With the spectrometer at 0°, we expect relevant background due to scattering off both the θ and φ slits, both set at 2°, which will be considerably more important for ^{208}Pb than ^{116}Sn.

The $E0$ distributions obtained in this work for ^{116}Sn, ^{144}Sm, and ^{208}Pb are in good agreement with those from the earlier analysis reported in Ref. [11] as can be seen in Fig. 10, though there are differences in strength as the earlier work used the deformed potential model. The normalization of the $E1$ distributions reported by Clark, Lui, and Youngblood [13] was off by a factor of 3 because the Harakeh and Dieperink [23] sum rule used is for only one magnetic substate. The distributions for ^{116}Sn and ^{208}Pb from Ref. [13], renormalized by this factor of 3, are compared to those from

TABLE II. Parameters obtained for the GMR.

	This work			Youngblood *et al.*[a]	Osaka[b]		
	m_1/m_0 (MeV)	Γ (MeV)	EWSR %	m_1/m_0 (MeV)	m_1/m_0 (MeV)	Γ (MeV)	EWSR %
^{116}Sn	15.85±0.20	5.27±0.25	112±15	16.07±0.12			
^{144}Sm	15.40±0.30	3.40±0.20	92±12	15.39±0.28	15.4±0.1	3.9±0.2	84±5
^{208}Pb	13.96±0.20	2.88±0.20	99±15	14.17±0.28	13.5±0.2	3.6±0.4	76±5

[a]Reference [11].
[b]References [15,16].

the present work in Fig. 11. In both nuclei the present analysis shows considerably more $E1$ strength and shows the $E1$ strength extending to higher excitation energy. This difference is due to the lower continua used for the spectra taken at 0° in the present analysis. The continua used in Ref. [13] corresponds closely to the highest continuum shown in the 1.1° spectrum in Fig. 3 as can be seen in Fig. 1 of Ref. [13]. The ISGDR distributions are clearly quite sensitive to continuum choices, particularly for the 0° data and logically the results of Ref. [13] represent some lower limit of ISGDR strength. However the $E0$, $E2$, and $E3$ distributions are not so sensitive to continuum choices as can be seen by comparing the distributions for ^{116}Sn shown in Ref. [13] with those from this work.

The properties of the GMR, GQR, ISGDR, and HEOR obtained in this work are given in Tables II–VI. The values in Tables II–V for the GMR, GQR, and HEOR are multipole moments obtained from the strength distributions. The full width at half maximum (FWHM), Γ was obtained by multiplying the rms width by 2.348 to convert to an equivalent Gaussian FWHM. The values for the ISGDR are the parameters obtained from a two Gaussian fit to the $E1$ distribution for each nucleus shown by the lines in Figs. 6 and 7. The errors given include systematic errors.

IV. DISCUSSION

The GMR energies obtained in this work for ^{116}Sn, ^{144}Sm, and ^{208}Pb are in agreement with those reported for the "slice analysis" by Youngblood, Lui, and Clark [11], as would be expected since this is for the most part a reanalysis of the same data. Hence the conclusions drawn in that work that a comparison with calculations using the Gogny interaction [26] leads to $K_{\mathrm{NM}}=231\pm5$ MeV are not changed. More recent relativistic calculations by Piekarewicz [27] for ^{208}Pb, and by Vretenar, Nikšić, and Ring [28] for ^{90}Zr, ^{116}Sn, ^{144}Sm, and ^{208}Pb, suggest that relativistic models with $K_{\mathrm{NM}}\sim 250-270$ MeV best reproduce GMR energies.

Experimental results for the GMR from work done at Osaka on ^{144}Sm [15] and ^{208}Pb [16] are shown in Table II. The GMR energies for ^{144}Sm agree, but the Osaka result for Pb is a little lower than our result. We note that Uchida *et al.* [16] report two different analyses for ^{208}Pb both giving 13.5 MeV for m_1/m_0 but obtaining 76%±5% and 58%±3% of the $E0$ EWSR in the peak. They also show a continuum of $E0$ strength extending up past $E_x=30$ MeV. The centroid of the entire $E0$ strength shown [16] in their Fig. 3 (estimated from the plot) is approximately 16.5 MeV. Their analysis does not subtract a continuum but rather assumes the entire

TABLE III. Parameters obtained for the ISGDR.

	Low energy peak										
	This work			Clark *et al.*[a]			Osaka[c]				
	E_x (MeV)	Γ (MeV)	EWSR %	E_x (MeV)	Γ (MeV)	EWSR[b] %	E_x (MeV)	Γ (MeV)	EWSR[d] %		
^{116}Sn	14.38±0.25	5.84±0.30	25±15	14.7±0.50	3.8±1.2	13±4					
^{144}Sm	14.00±0.30	8.0±0.60	32±15								
^{208}Pb	13.26±0.30	5.68±0.50	24±15	12.2±0.60	4.5±1.2	10±4	12.5±0.3	4.4±0.5	21±6		
	High energy peak										
				Total ISGDR				Total ISGDR			Total ISGDR
	E_x (MeV)	Γ (MeV)	EWSR %	EWSR %	E_x (MeV)	Γ (MeV)	EWSR[b] %	EWSR[b] %	E_x (MeV)	Γ (MeV)	EWSR[d] %	EWSR[d] %
^{116}Sn	25.50±0.60	12.0±0.6	61±15	88±20	23.0±0.60	8.7±1.2	33±5	46±11				
^{144}Sm	24.51±0.40	7.21±0.40	64±12	97+10−20								
^{208}Pb	22.20±0.30	9.39±0.35	88±15	114+12−25	19.9±0.8	5.9±1.4	38±7	48±9	22.5±0.3	10.9±0.9	107±31	128±40

[a]Reference [13].
[b]Reduced by factor of 3 from quoted value, see text.
[c]Reference [16].
[d]Includes 30% systematic error stated in Reference [16].

TABLE IV. Parameters obtained for the GQR.

	This Work			Youngblood *et al.*[a]			Groningen[b,c]		
	E_x (MeV)	Γ (MeV)	EWSR %	E_x (MeV)	Γ (MeV)	EWSR %	E_x (MeV)	Γ (MeV)	EWSR %
^{116}Sn	13.50±0.35	5.00±0.30	108±12	13.2±0.2	3.3±0.2	84±25	13.39±0.14	2.94±0.31	134±28
^{144}Sm	12.78±0.30	4.82±0.30	98±13	12.2±0.2	2.4±0.2	45±15	12.70±0.14	2.62±0.20	123±29
^{208}Pb	10.89±0.30	3.00±0.30	100±13	11.0±0.2	2.7±0.3	105±25	10.9±0.3[a]	3.1±0.3[a]	120−170[a]

[a]Reference [25].
[b]Reference [34].
[c]Reference [33].

spectrum can be explained by a sum of multipole transitions. They also argue that their spectra contain no experimental background. However, both the ^{144}Sm and ^{208}Pb multipole distributions all contain, in addition to the GR peaks, a continuous component extending up to at least E_x=32 MeV which they do not explain. In several cases the integrated strength would considerably exceed the EWSR. They do speculate that they have some other process which appears as an L=1 component in their spectra. The continuous $E0$ and $E2$ strength above the GR peaks in their results would suggest these other processes might also emulate $E0$ and $E2$ strength. There is no such continuous component in our peak analysis, in part because it has been subtracted as part of the continuum.

The Osaka results for the ISGDR in ^{208}Pb are compared to our results in Table III. Their energy and width are slightly lower for the lower component while our energy and width are slightly lower for the upper component. The strengths agree within the errors. Their data at both low and high excitation deviates considerably from their fits, and at high excitation the $E1$ strength appears to be increasing up to the highest energy shown. The energy reported by Davis *et al.* [9] for the upper component (22.4±0.5 MeV) is consistent with both measurements, but Davis *et al.* report a width of 3.5±0.5 MeV, nearly a factor of 3 less than either our result or that from Osaka. Morsch *et al.* [8] could not definitively identify the ISGDR, but suggested a peak at 21.4±0.5 MeV with a width of 5.65±0.6 MeV was due to the ISGDR. Our experimental strength functions are compared to Hartree-Fock–random-phase approximation (HF-RPA) calculations of Colo *et al.* [29] and relativistic calculations of Vretenar *et al.* [30] in Fig. 12 using interactions that result in K_{NM} =215 MeV (Colo *et al.*) and 211 MeV (Vretenar *et al.*). Continuum RPA calculations for ^{208}Pb by Hamamoto and Sagawa [31] using SKM$\star$ (K_{NM}=217 MeV) give results almost identical to the Colo *et al.* result. For ^{116}Sn, ^{144}Sm, and ^{208}Pb, the observed low energy component is several MeV higher than predicted. The high energy component is in each case somewhat lower than predicted, suggesting a K_{NM} somewhat less than 211 MeV whereas the GMR data is best explained with $K_{\mathrm{NM}}\sim$230 MeV. The peak positions from the relativistic RPA calculations by Vretenar *et al.* are similar to those from the Colo *et al.* and Hamamoto and Sagawa calculations but the strengths of the two peaks obtained by Vretenar *et al.* are in better agreement with the ^{208}Pb data. Ma *et al.* [32] compared GMR and ISGDR results from several parametrizations corresponding to $K_{NM}\sim$210−540 in the relativistic random phase approximation, and concluded that the energy of the GMR's in ^{144}Sm and ^{208}Pb were consistent with $K_{\mathrm{NM}}\sim$250−270 MeV. However all of the calculations of ^{208}Pb, including another relativistic calculation by Piekarewicz [27] all resulted in energies for the ISGDR in ^{208}Pb from $E_x\sim$24.5−25.5 MeV compared to our result of 22.2±0.3 MeV and the Osaka result [16] of 23.0±0.3 MeV.

The GQR has been studied extensively [3], and there are several earlier reports of the HEOR [3], however in these studies the parameters for the resonances were obtained assuming the different GR components can be represented by Gaussian peaks, whereas our analysis makes no assumption about the shape of the strength distributions. RPA-HF calculations [3] show the strength of each multipole distributed in several components, which would not inherently result in a symmetric shape for the strength of that multipole. Furthermore, most of these earlier studies used the deformed poten-

TABLE V. Parameters obtained for the HEOR.

	This work			Clark *et al.*[a]			Carey *et al.*[b]			Yamagata *et al.*[c]	
	E_x (MeV)	Γ (MeV)	EWSR %	E_x (MeV)	Γ (MeV)	EWSR %	E_x (MeV)	Γ (MeV)	EWSR %	E_x (MeV)	EWSR %
^{116}Sn	23.3±0.8	10.9±0.6	70±12	21.8±0.5	7.1±0.5	67±10	22.9±1.1	6.5±1.0	22±6	24.4±1.5	∼74
^{144}Sm	19.8±0.5	9.6±0.7	78±12							23.0±2.0	
^{208}Pb	19.6±0.5	7.4±0.6	70±14				19.1±1.1	5.3±0.8	20±6	20.5±1.0	78±15

[a]Reference [35].
[b]Reference [36].
[c]Reference [37].

TABLE VI. Parameters obtained for ^{154}Sm.

	Lower peak			Upper peak		
	E_x (MeV)	Γ (MeV)	EWSR %	E_x (MeV)	Γ (MeV)	EWSR %
GMR[a]	11.05±0.05	3.2±0.1	32±2	15.17±0.05	4.0±0.1	80±5
ISGDR[b]	13.3±0.3	7.0±0.3	44±7	23.5±0.3	11.8±0.5	67±15
GQR[b]	12.1±0.3	5.7±0.3	97±14			
HEOR[b]	18.5±0.5	10.0±0.6	74±15			

[a]Gaussian fits, errors do not include systematic errors.
[b]Moments obtained from the distribution.

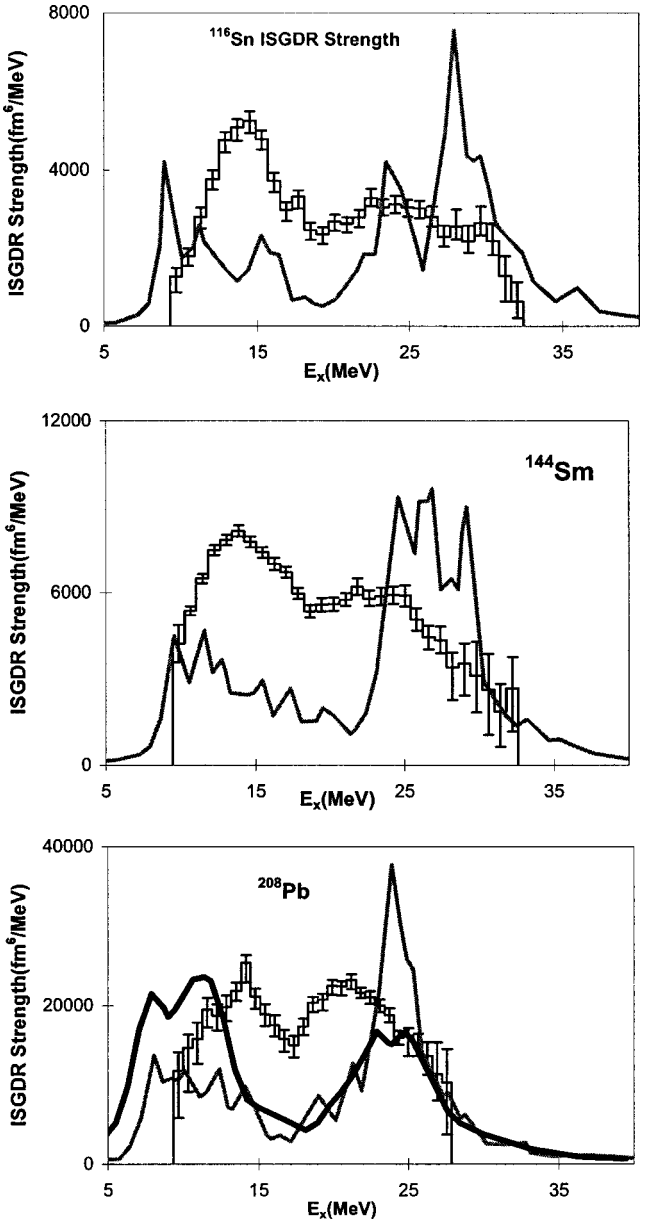

FIG. 12. The $E1$ strength distributions obtained (shown by the histograms) for ^{116}Sn, ^{144}Sm, and ^{208}Pb are compared to calculations by Colo *et al.* [29] shown by the thick gray lines and by Vretenar, Wandelt, and Ring [30] shown by the thick black line.

tial model which is known to not reproduce electromagnetic B(EL) values [17]. Below we describe comparisons with other works where our results quoted are moments obtained from the slice analysis with folding model calculations and the other results are parameters from Gaussian peak fits and a deformed potential analysis, so some differences would be expected.

Our results for the GQR are compared to two other studies [33,34] in Table IV. The excitation energies and strengths obtained in the three studies are in agreement for ^{116}Sn and ^{208}Pb, however the excitation energy and strength reported by Youngblood *et al.* [25] for the GQR in ^{144}Sm was somewhat lower than the present result and that reported by Sharma *et al.* [33]. The widths we obtain (rms widths converted to a Gaussian equivalent FWHM) are substantially higher, in part because the GQR peak differs somewhat from a Gaussian shape.

Our results for the HEOR are compared with three other studies [35–37] in Table V. For ^{116}Sn the energies are in agreement, and except for the 800 MeV proton study [36] which reported only 22% of the EWSR, each study found approximately 75% of the EWSR expected in the HEOR [3]. Bonin *et al.* [38] also reported $E3$ strength centered $\sim$23 MeV in ^{116}Sn with both 340 and 480 MeV α scattering but identified less than 15% of the EWSR. The excitation energy we obtain for ^{144}Sm is lower than reported by Yamagata *et al.* [37], however Yamagata *et al.* do not report a strength or width for the HEOR in ^{144}Sm. The energies obtained for the HEOR in ^{208}Pb are in agreement, but the 800 MeV proton work identified only 20% of the EWSR.

^{154}Sm has an axial deformation with $\beta\sim0.3$ and the effects of this ground state deformation on the isoscalar monopole and quadrupole giant resonances have been investigated both experimentally [39] and theoretically [40] in several works. Nishizaki and Ando [41] in a fluid dynamical description also explored the behavior of the ISGDR and HEOR in a deformed nucleus and Itoh *et al.* [15] showed $E1$ and $E3$ strength extracted in the GR region in a 400 MeV α experiment on ^{154}Sm, but did not do a detailed comparison with the Nishizaki and Ando work. The $E0$ and $E2$ strength distributions we obtain for ^{154}Sm are shown in Fig. 13. The GMR clearly consists of two components and a two peak fit yielding the parameters in Table VI is shown in the middle panel. In the top panel, calculations using the parameters predicted by Abgrall *et al.* [40], and by Nishizaki and Ando [41] (for $m^*/m=0.7$ and $F_0=-0.45$) are shown superimposed on the

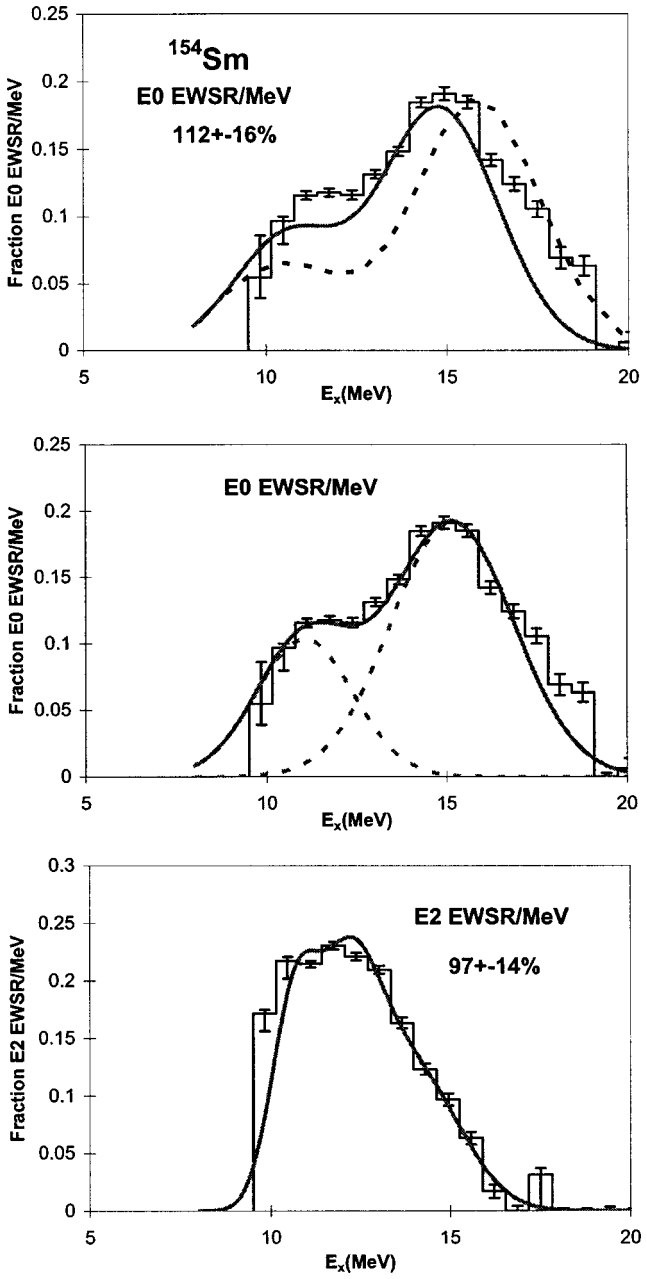

FIG. 13. The $E0$ strength distribution obtained for ^{154}Sm is shown by the histograms in the top two panels. In the top panel, a calculation using the parameters of Abgrall *et al.* [40] is shown by the dashed line and one using the parameters of Nishizaki and Ando [41] is shown by the gray line. A two Gaussian fit to the $E0$ distribution with the parameters in Table VI is shown in the middle panel. The $E2$ strength distribution obtained for ^{154}Sm is shown by the histogram in the bottom panel and a calculation using the parameters of Nishizaki and Ando [41] is shown by the gray line.

data. The widths of the peaks were chosen to best represent the data. It can be seen that the fluid dynamical calculations give a fairly good representation of the data. A calculation for the GQR strength using the same Nishizaki and Ando prediction is shown superimposed on the GQR data in the bottom panel and also gives a good representation of the data.

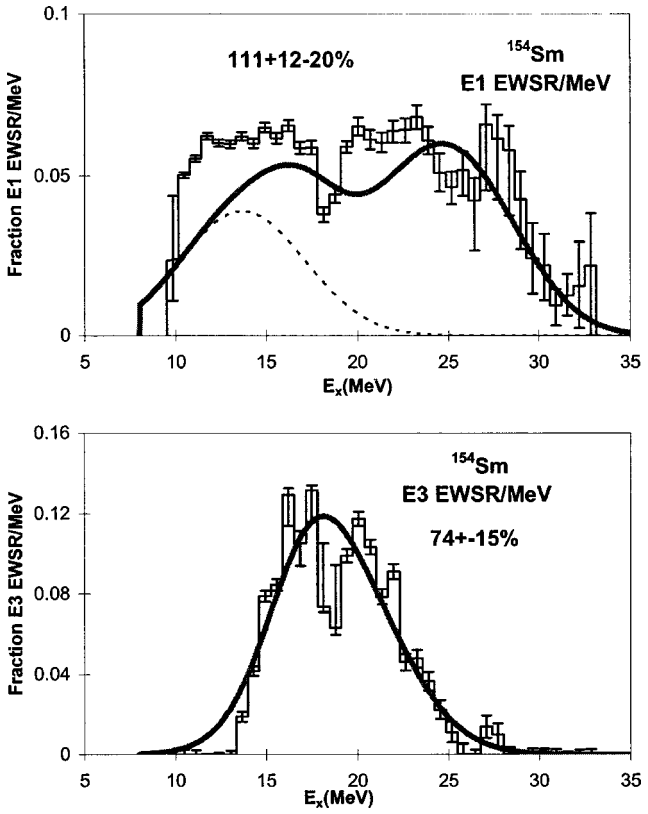

FIG. 14. The $E1$ ($E3$) strength distribution obtained for ^{154}Sm is shown by the histogram in the top (bottom) panel. Calculations using the parameters of Nishizaki and Ando [41] are shown by the gray lines. The dashed line is the shifted ^{144}Sm distribution for the lower component of the ISGDR as described in the text. The gray line for the $E1$ distribution includes the contribution illustrated by the dashed line.

The isoscalar $E1$ and $E3$ distributions obtained in ^{154}Sm are shown in Fig. 14. As for the other nuclei, the $E1$ strength is divided into two components, though in ^{154}Sm the components are definitely not Guassian in shape. There is some disagreement on the origin of the lower component of the $E1$ strength [27,29–31], but the upper component is expected to be the compression mode, which is treated in the Nishizaki and Ando [41] calculations. A calculation using the parameters from Nishizaki and Ando, with the strength normalized to the experimental strength of the upper component, and the lower component taken from the ^{144}Sm analysis (shifted in energy with $1/A^{1/3}$) is shown superimposed on the data. The calculation gives a reasonable representation of the high energy portion of the data. It would appear that the lower component of the ISGDR is both shifted down in energy and itself split into more than one component in ^{154}Sm relative to ^{144}Sm. The distribution of HEOR strength calculated using the splitting predicted in Nishizaki and Ando calculation is shown superimposed on the data in the bottom panel of Fig. 13. Except for the dip in the middle of the data, the calculation gives an excellent representation of the data.

V. CONCLUSIONS

Within errors, all of the isoscalar $E0$, $E1$, $E2$, and $3\hbar\omega$ $E3$ giant resonance strength was located in ^{116}Sn, ^{144}Sm, ^{154}Sm,

and ^{208}Pb. The distributions of $E0$ and $E2$ strength are in agreement with previous works, and in particular with the location of the GMR reported in Ref. [11] which led to the conclusion that $K_{NM} \sim 231$ MeV. The ISGDR is seen to consist of two components, the upper component (presumably) being the compression mode [27,29,30]. Microscopic predictions for ^{116}Sn, ^{144}Sm, and ^{208}Pb with RPA-HF calculations [29,31] with the SGII ($K_{NM}=215$ MeV) and SKM$\star$ ($K_{NM}=217$ MeV) interactions and relativistic calculations [27,30] for ^{208}Pb using the NLC ($K_{NM}=224$ MeV) and NL1 parametrization ($K_{NM}=211.7$ MeV) all show the compression mode peak higher than the experimental peak by 1–2 MeV and the lower component at a lower excitation than the experimental peak. Studies using the relativistic random phase approximation [27,28,32] were able to reproduce GMR energies with parametrizations having $K_{NM} \sim 250-270$ MeV, but the predicted energy of the ISGDR compression mode is also 1–2 MeV above experimental values. By comparison to the results we reported in Ref. [13], it is seen that the experimental ISGDR strength extracted from the data is quite sensitive to the continuum chosen. This is in part because the cross section for $E1$ excitation becomes very small as the excitation energy increases [42]. It is possible that there is unobserved $E1$ strength at higher excitation, which could shift the centroid of the compression mode peak somewhat, however most of the $E1$ strength in ^{208}Pb is accounted for. The 400 MeV α experiments [15,16] have a large continuous $E1$ component, and do not help resolve this issue.

For the deformed nucleus ^{154}Sm, the splitting of the GMR is clearly apparent in the $E0$ strength distribution. The $E1$ distribution is also qualitatively different than that for the spherical nuclei, with almost flat top distributions for both components of the ISGDR, compared to Gaussian distributions for the spherical nuclei. This same behavior can be seen in the distribution obtained for ^{154}Sm by Itoh *et al.* [15]. Except for the lower component of the ISGDR, all of the ^{154}Sm multipole distributions are reasonably well reproduced assuming the splitting for each multipole predicted with the fluid dynamical calculations of Nishizaki and Ando [41]. The existence of this lower component of the ISGDR was not known at the time of their calculations.

ACKNOWLEDGMENTS

This work was supported in part by the U.S. Department of Energy under Grant No. DE-FG03-93ER40773 and by The Robert A. Welch Foundation.

[1] R. Pitthan and Th. Walcher, Phys. Lett. **36B**, 563 (1971); M. B. Lewis and F. E. Bertrand, Nucl. Phys. **A196**, 337 (1972).
[2] D. H. Youngblood, J. Moss, C. M. Rozsa, J. D. Bronson, A. D. Bacher, and D. R. Brown, Phys. Rev. C **13**, 994 (1976).
[3] A. van der Woude, Int. Rev. Nucl. Phys. **7**, 100 (1991); J. Speth and J. Wambach, *ibid.* **7**, 2 (1991).
[4] J. M. Moss, D. H. Youngblood, C. M. Rozsa, D. R. Brown, and J. D. Bronson, Phys. Rev. Lett. **37**, 816 (1976); Phys. Rev. C **18**, 741 (1978).
[5] J. P. Blaizot, Phys. Rep. **64**, 171 (1980).
[6] D. H. Youngblood, C. M. Rozsa, J. M. Moss, D. R. Brown, and J. D. Bronson, Phys. Rev. Lett. **39**, 1188 (1977).
[7] S. Shlomo and D. H. Youngblood, Phys. Rev. C **47**, 529 (1993), and references therein.
[8] H. P. Morsch, M. Rogge, P. Turek, and C. Mayer-Boricke, Phys. Rev. Lett. **45**, 337 (1980).
[9] B. F. Davis *et al.*, Phys. Rev. Lett. **79**, 609 (1997).
[10] S. Stringari, Phys. Lett. **108B**, 232 (1982).
[11] D. H. Youngblood, H. L. Clark, and Y.-W. Lui, Phys. Rev. Lett. **82**, 691 (1999).
[12] D. H. Youngblood, Y.-W. Lui, and H. L. Clark, Phys. Rev. C **60**, 067302 (1999).
[13] H. L. Clark, Y.-W. Lui, and D. H. Youngblood, Phys. Rev. C **63**, 031301(R) (2001).
[14] D. H. Youngblood, Y.-W. Lui, and H. L. Clark, Phys. Rev. C **65**, 034302 (2002); **63**, 067301 (2001); **61**, 067307 (2000); **60**, 014304 (1999); **55**, 2811 (1997).
[15] M. Itoh *et al.*, Phys. Lett. B **549**, 58 (2002).
[16] M. Uchida *et al.*, Phys. Lett. B **557**, 12 (2003).
[17] J. R. Beene, D. J. Horen, and G. R. Satchler, Phys. Lett. B **344**, 67 (1995).
[18] K. van der Borg, M. N. Harakeh, and A. van der Woude, Nucl. Phys. **A365**, 243 (1981).
[19] G. R. Satchler and Dao T. Khoa, Phys. Rev. C **55**, 285 (1997).
[20] H. L. Clark, Y.-W. Lui, and D. H. Youngblood, Phys. Rev. C **57**, 2887 (1998).
[21] H. L. Clark, Y.-W. Lui, and D. H. Youngblood, Nucl. Phys. **A687**, 80c (2000).
[22] D. H. Youngblood, Y.-W. Lui, and H. L. Clark, Phys. Rev. C **55**, 2811 (1997).
[23] M. N. Harakeh and A. E. L. Dieperink, Phys. Rev. C **23**, 2329 (1981).
[24] S. S. Dietrich and B. L. Berman, At. Data Nucl. Data Tables **38**, 199 (1988).
[25] D. H. Youngblood, P. Bogucki, J. D. Bronson, U. Garg, Y.-W. Lui, and C. M. Rozsa, Phys. Rev. C **23**, 1997 (1981).
[26] J. Blaizot, J. F. Berger, J. Dechargé, and M. Girod, Nucl. Phys. **A591**, 435 (1995).
[27] J. Piekarewicz, Phys. Rev. C **64**, 024307 (2001).
[28] D. Vretenar, T. Nikšić, and P. Ring, Phys. Rev. C **68**, 024310 (2003).
[29] G. Colo, N. Van Giai, P. F. Bortignon, and M. R. Quaglia, Phys. Lett. B **485**, 362 (2000).
[30] D. Vretenar, A. Wandelt, and P. Ring, Phys. Lett. B **487**, 334 (2000).
[31] I. Hamamoto and H. Sagawa, Phys. Rev. C **66**, 044315 (2002).
[32] Zhong-yu Ma, Nguyen Van Giai, A. Wandelt, D. Vretenar, and P. Ring, Nucl. Phys. **A686**, 173 (2001).
[33] M. M. Sharma, W. T. A. Borghols, S. Brandenburg, S. Crona, A. Van der Woude, and M. N. Harakeh, Phys. Rev. C **38**, 2562 (1988).
[34] S. Brandenberg *et al.*, Nucl. Phys. **A466**, 29 (1987).

[35] H. L. Clark, D. H. Youngblood, and Y.-W. Lui, Phys. Rev. C **54**, 72 (1996).
[36] T. A. Carey *et al.*, Phys. Rev. Lett. **45**, 239 (1980).
[37] T. Yamagata, S. Kishimoto, K. Yuasa, K. Iwamoto, B. Saeki, M. Tanaka, T. Fukuda, I. Miura, and H. Ogata, Phys. Rev. C **23**, 937 (1981).
[38] B. Bonin *et al.*, Nucl. Phys. **A430**, 349 (1984).
[39] T. Kishimoto, J. M. Moss, D. H. Youngblood, J. D. Bronson, C. M. Rozsa, D. R. Brown, and A. D. Bacher, Phys. Rev. Lett. **35**, 552 (1975); U. Garg, P. Bogucki, J. D. Bronson, Y.-W. Lui, C. M. Rozsa, and D. H. Youngblood, *ibid.* **45**, 1670 (1980).
[40] Y. Abgrall, B. Morand, E. Caurier, and N. Grammaticos, Nucl. Phys. **A346**, 431 (1980), and references therein.
[41] S. Nishizaki and K. Ando, Prog. Theor. Phys. **73**, 889 (1985).
[42] S. Shlomo and A. I. Sanzhur, Phys. Rev. C **65**, 044310 (2002).